

How a cofactor-free protein environment lowers the barrier to O₂ reactivity

Received for publication, October 5, 2018, and in revised form, January 1, 2019 Published, Papers in Press, January 2, 2019, DOI 10.1074/jbc.RA118.006144

Melodie M. Machovina[‡], Emerald S. Ellis[‡], Thomas J. Carney[§], Fikile R. Brushett[¶], and Jennifer L. DuBois^{‡1} From the [‡]Department of Chemistry and Biochemistry, Montana State University, Bozeman, Montana 59715-3400 and the Departments of § Materials Science and Engineering and ¶ Chemical Engineering, Massachusetts Institute of Technology, Cambridge, Massachusetts 02139-4307

Edited by F. Peter Guengerich

Molecular oxygen (O2)-utilizing enzymes are among the most important in biology. The abundance of O_2 , its thermodynamic power, and the benign nature of its end products have raised interest in oxidases and oxygenases for biotechnological applications. Although most O2-dependent enzymes have an absolute requirement for an O₂-activating cofactor, several classes of oxidases and oxygenases accelerate direct reactions between substrate and O2 using only the protein environment. Nogalamycin monooxygenase (NMO) from Streptomyces nogalater is a cofactor-independent enzyme that catalyzes rate-limiting electron transfer between its substrate and O2. Here, using enzymekinetic, cyclic voltammetry, and mutagenesis methods, we demonstrate that NMO initially activates the substrate, lowering its pK_a by 1.0 unit ($\Delta G^* = 1.4 \text{ kcal mol}^{-1}$). We found that the oneelectron reduction potential, measured for the deprotonated substrate both inside and outside the protein environment, increases by 85 mV inside NMO, corresponding to a $\Delta\Delta G^{0}$ of 2.0 kcal mol⁻¹ (0.087 eV) and that the activation barrier, ΔG^{\dagger} , is lowered by 4.8 kcal mol⁻¹ (0.21 eV). Applying the Marcus model, we observed that this suggests a sizable decrease of 28 kcal mol $^{-1}$ (1.4 eV) in the reorganization energy (λ), which constitutes the major portion of the protein environment's effect in lowering the reaction barrier. A similar role for the protein has been proposed in several cofactor-dependent systems and may reflect a broader trend in O₂-utilizing proteins. In summary, NMO's protein environment facilitates direct electron transfer, and NMO accelerates rate-limiting electron transfer by strongly lowering the reorganization energy.

Reactions between organic molecules and O₂ power aerobic life. Although O2 is a thermodynamically powerful oxidant, well-described kinetic (1, 2) and thermodynamic (2, 3) barriers render it largely inert under ambient conditions. This lack of apparent reactivity protects biological molecules from unwanted oxidations. To harness its oxidizing power, nature has evolved several organic and metallocofactors capable of binding and donating electrons to O_2 (4-8). The partially reduced forms of O₂ (superoxide or peroxide anions) are both

activated for oxidizing exogenous substrates and sheltered inside proteins, where they may access substrates selectively

Several classes of oxidases and oxygenases are known that directly catalyze reactions between substrates and O2 in a cofactor-independent manner (10) and are broadly termed cofactor-independent oxidases and oxygenases. Examples of these are the antibiotics biosynthesis monooxygenases (ABMs),² a large family of enzymes involved in the synthesis of bacterial antibiotics. These catalyze oxidations and oxygenations of mono-, tri-, and tetracycline natural products through the direct interaction of the substrate and O_2 (11–16).

Working with a member of this class known as nogalamycin monooxygenase (NMO), we previously compared the mechanisms of the catalyzed and uncatalyzed reactions of dithranol, a tricyclic anthraquinol analog of 12-deoxynogalonic acid (Scheme 1) (17). With the substrate in its deprotonated, monoanionic form (dithranol⁻), we observed rate-limiting electron transfer in both the uncatalyzed and catalyzed reactions, where the presence of the protein led to an approximate 2000-fold increase in the reaction rate (17). Although modest, this increase is nonetheless of interest, because it suggests ways in which the protein environment alone can accelerate reactions with O2, in both natural and designed enzymes that exploit this abundant, "green" oxidant.

Here, we have begun to quantify how the enzyme activates both the organic substrate and O2. Because the rate-limiting step is an electron transfer, Marcus theory can be applied. The Marcus model states that the activation barrier (ΔG^{\dagger}) for electron transfer is a function of how the chemical environment influences the free energy difference (ΔG^0) between the ground (reduced) and $1e^-$ oxidized states, and the energy required to reorganize the reactants and solvent in the excited state (λ) . Because of the simplicity of our system—a small, structurally characterized 34-kDa enzyme that lacks a cofactor-and our ability to study the uncatalyzed reaction in parallel, we were able to use the Marcus model to directly assess how the protein

This work was supported by National Science Foundation Grant MCB1715176. The authors declare that they have no conflicts of interest with the contents of this article.

This article contains Figs. S1-S7.

To whom correspondence should be addressed. Tel.: 406-994-2844; E-mail: jennifer.dubois1@montana.edu.

² The abbreviations used are: ABM, antibiotics biosynthesis monooxygenase; NMO, nogalamycin monooxygenase; ME, 2-methoxyethanol; CAPS-ME, 0.1 M CAPS, 0.3 m NaCl, 36% (v/v) 2-methoxyethanol; CV, cyclic voltammetry; SHE, standard hydrogen electrode; PCET, proton-coupled electron transfer; ES, enzyme-substrate; BES, 2-[bis(2-hydroxyethyl)amino]ethanesulfonic acid; Tricine, N-[2-hydroxy-1,1-bis(hydroxymethyl)ethyl]glycine; CHES, 2-(cyclohexylamino)ethanesulfonic acid; CAPS, 3-(cyclohexylamino)propanesulfonic acid.

Protein-mediated O2 activation

Scheme 1. Proposed pathway for the oxygenation of dithranol and 12-deoxynogalonic acid. Dithranol, the substrate analog of 12-deoxynogalonic acid (12-deoxynogalonic acid-specific substituents in *gray*), transfers an electron to O₂, forming a dithranyl radical and superoxide pair in a step that prior work suggests is rate-limiting (*RLS*; *Step 1*). This occurs faster under basic conditions where the starting substrate is an anion. In *Step 2*, the radicals recombine to form a peroxy adduct that breaks down to dithranone and water.

environment lowers the barrier to electron transfer between a simple substrate and O_2 .

Results

Pure WT and mutant NMO were prepared in high yields

His₆-NMO was purified as a homodimer in average yields of 50 mg/liter of culture for WT, 20 mg/liter for the N18A, and 30 mg/liter for the N63A variant. Pure enzyme had a measured subunit molecular mass of 16.85 kDa (MS); calculated 16.98 kDa. The discrepancy was attributed to loss of part of the histidine tag before or during MS analysis. Typical values for the specific activity of freshly prepared enzyme with saturating (\geq 5 times K_m) dithranol in air-saturated buffer, consisting of 0.1 M CAPS, 0.3 M NaCl, 36% (v/v) 2-methoxyethanol (CAPS-ME), pH 9.8, 25 °C, were 47 \pm 7 μM min⁻¹ μM⁻¹ NMO (WT), 0.41 \pm 0.1 μM min⁻¹ μM⁻¹ NMO (N18A), and 0.15 \pm 0.006 μM min⁻¹ μM⁻¹ NMO (N63A). The enzyme retained full activity for at least 25 min in the 2-methoxyethanol (ME) containing buffer, after which activity began to decline.

NMO lowers the pK_a of the bound substrate

The p K_a of free dithranol in solution is 7.9 ± 0.4 , but when bound to WT NMO, the value is lowered by $1.0 \text{ p}K_a$ unit to 6.9 ± 0.2 (Fig. 1). This suggests that NMO plays a role in promoting formation of the reactive dithranol⁻ at physiological pH and temperature (pH 7, 25 °C), an effect corresponding to $\Delta G^{0'} = 1.4 \text{ kcal mol}^{-1}$ (18). Previously, we saw that catalytic activity was significantly reduced in two active site asparagine mutants of NMO (17). To probe whether these are involved in lowering the substrate p K_a , pH titrations were carried out for the enzyme–substrate (ES) complexes of the N18A and N63A variants, yielding values of 7.8 ± 0.2 and 7.7 ± 0.1 , respectively (Fig. S1). Hence, both Asn-18 and Asn-63 appear to be involved in facilitating the deprotonation reaction.

The uncatalyzed oxygenation of dithranol has a modest barrier

A discontinuous HPLC method was used to monitor the initial rate of dithranol $^-$ oxygenation under pseudo-first order conditions (constant O_2 concentration, pH 9.8, 25 °C). Dithranone, dithranol, and bisanthrone have well-resolved peaks with retention times of 2.3, 2.7, and 3.2 min, respectively (Fig. S2).

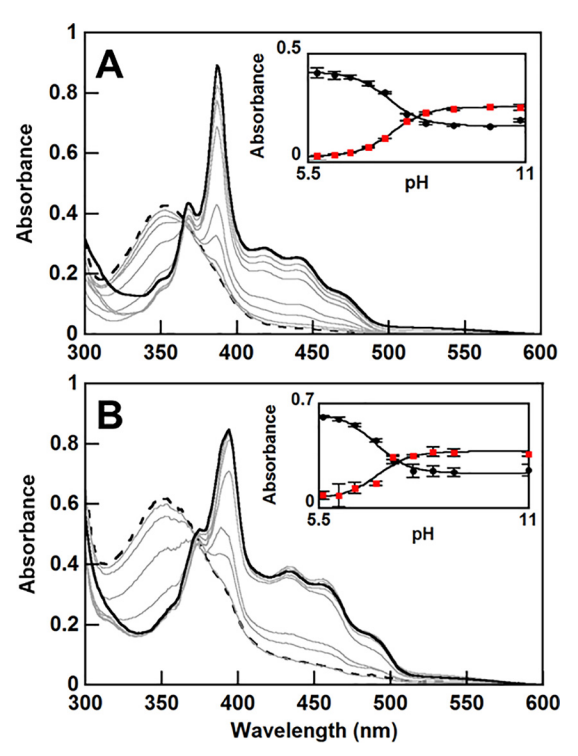


Figure 1. NMO lowers the p K_a **of dithranol.** Spectrophotometric titrations of 50 μM dithranol (A) or the NMO– dithranol complex (B, 100 μM dithranol + 150 μM WT NMO) in buffer over pH 5.8–10.9 reveal that NMO lowers the p K_a by 1.0 unit. All pH titrations were performed by a discontinuous method using a different buffer for each pH because of instability of the enzyme when concentrated acid or base is added. See methods for buffers used. The pH 5.8 (dotted black line) and pH 10.9 spectra (solid black) are highlighted. Insets, the absorbance at 354 nm (black circles) and 440 nm (red squares) is plotted versus pH and fit to a sigmoidal curve to obtain values for p K_a (Equation 3): 7.9 ± 0.4 (free dithranol) and 6.9 ± 0.2 (NMO– dithranol complex). Error bars represent ±1 standard deviation of three or more independent titrations.

The rate of dithranol oxygenation increased with O_2 concentration, with the highest attainable dissolved $[O_2]$ (935 μ M) resulting in exponential loss of the initial 200 μ M dithranol within 2.5 min (Fig. S3). In each case, dithranone formed in a 1:1 ratio with dithranol Because of the slow oxidation of dithranol, especially at low temperatures and $[O_2]$, the method of initial rates was used to find k' (17). [dithranol]_t/[dithranol]_{initial} of the initial, linear portion of the curve was plotted versus time (Fig. 2), yielding a slope equal to k' (Equation 8), where k' is equal to the rate constant, k, times $[O_2]$ (Equation 8).



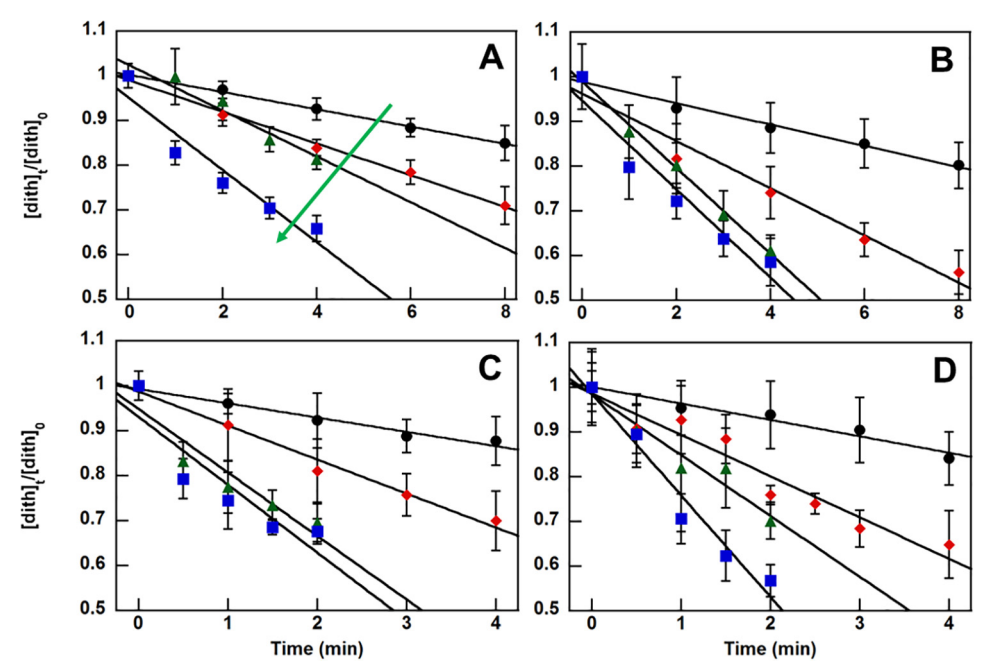


Figure 2. Second-order rate constants for the uncatalyzed reaction between dithranol and O₂ were measured as a function of increasing temperature. The method of initial rates for pseudo-first order reactions was used to determine k' for dithranol (dith) oxidation at 210 – 280 (black circles), 460 – 550 (red diamonds), 710 – 850 (green triangles), and 940 – 1175 (blue squares) μ M O₂ in CAPS-ME, pH 9.8 at 10 °C (A), 15 °C (B), 20 °C (C), and 25 °C (D). The reactions were stirred under constant $[O_2]$, with the green arrow showing increasing $[O_2]$. The slope of the line for $[dith]_1$ / $[dith]_0$ versus time gives k' (Equation 8). Error bars represent ± S.D. of three or more independent experiments for each time point.

Plotting measured k' values $\mathit{versus}\left[\mathrm{O}_2\right]$ (Fig. S4) yielded lines of increasing steepness as both [O2] and temperature were increased (Fig. 2 and Fig. S4). In (k) was then plotted as a function of temperature (1000 R^{-1} T^{-1}), using Equation 5, which yielded a negative linear relationship from which $\epsilon_a = 15 \pm 1$ kcal mol $^{-1}$ and the pre-exponential term, $\ln (A) = 26 \pm 2$, were determined (Fig. 3 and Table 1).

NMO lowers the activation barrier for oxidizing dithranol

Oxygenation of dithranol in the presence of NMO is significantly faster than the uncatalyzed reaction and similarly increases in rate with [O₂] (Fig. 4, Table 1, and Fig. S5). Analogous to the uncatalyzed reaction, the rate of dithranol oxidation with NMO also increases as temperature is increased (Fig. 4). For the enzymatic reaction, $k_{cat}/K_m(O_2)$ is used in place of a second-order rate constant, as described under "Experimental procedures" and in prior work by our group and others (5, 17, 19). The plot of $\ln (k_{\text{cat}}/K_m(O_2))$ versus 1000 R^{-1} T^{-1} has a negative linear slope, giving an activation energy $\epsilon_a = 6.0 \pm 1$ kcal mol⁻¹ and ln (A) = 19 ± 3 (Fig. 3 and Table 1). The activation energy is lower than the uncatalyzed reaction by \sim 2.5-fold.

Temperature dependence of NMO mutants

Both N18A and N63A show significantly reduced catalytic efficiency compared with WT NMO (Fig. S6 and Table 1). We examined the temperature dependence of $k_{\text{cat}}/K_m(O_2)$ for these mutants to measure their activation energies. However, neither mutant exhibited any kinetic sensitivity in changes to temperature (Fig. S6). We were therefore unable to use the Arrhenius relationship to determine the activation barriers for these mutants.

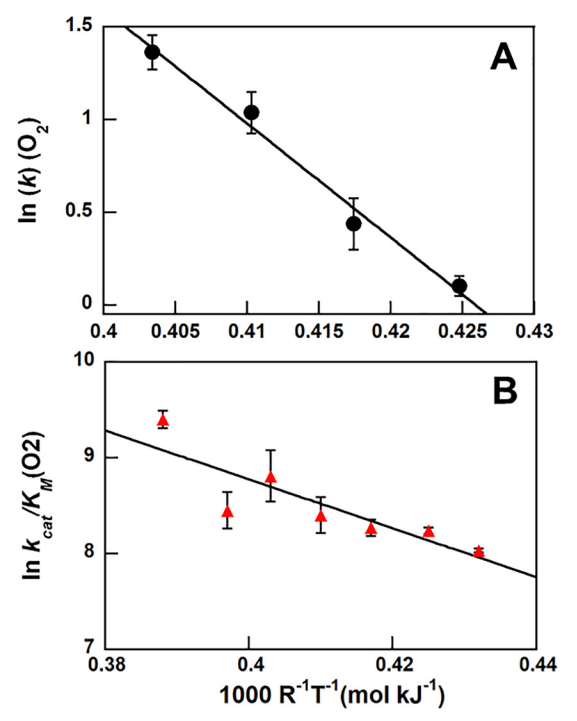


Figure 3. Arrhenius plots were used to measure the activation barriers for NMO-catalyzed and uncatalyzed dithranol oxygenation. The natural log of either ln (k) (O₂) (A, uncatalyzed) or (B, k_{cat}/K_m) (O₂) (catalyzed) determined from Figs. 2 and 3 and Fig. S4 at variable temperatures was plotted as a function of $1000 R^{-1} T^{-1}$ and fit to a linear equation (Equation 5). The activation energy for the uncatalyzed reaction is 15 \pm 1 kcal mol⁻¹, whereas that of the NMO catalyzed reaction is 6.0 \pm 1 kcal mol⁻¹. Error bars represent \pm S.D. of three or more runs.

The protein environment does not significantly change the free energy, $\Delta G^{0\prime}$, for dithranol oxidation. Oxidation peak potentials (E_p) for the one electron oxidation of dithranol to



Protein-mediated O₂ activation

Table 1 Kinetic and thermodynamic data for oxidation of dithranol and its complex with WT and variant NMO ND, not determined.

	Dithranol ⁻ (uncatalyzed)	WT NMO-dithranol ⁻	N18A NMO-dithranol	N63A NMO-dithranol
$k(O_2)$ or $k_{cat}/K_m(O_2)^{a,b}$	3.4 ± 0.2	7400 ± 300	90 ± 60	32 ± 10
ϵ_a (kcal mol ⁻¹)	15 ± 1	6.0 ± 1	ND	ND
$\ln A^{a,b,c}$	26 ± 2	19 ± 3	ND	ND
ΔH^{\dagger} (kcal mol ⁻¹) ^d	14 ± 1	5.4 ± 1	ND	ND
ΔS^{\dagger} (kcal mol ⁻¹ K ⁻¹) ^{a,e}	0.0013	0.013	ND	ND
ΔG^{\sharp} (kcal mol ⁻¹) a,f	14 ± 1	9.2 ± 1	ND	ND
$E^{0'}$ (V) vs. Ag/AgCl ^{g,h}	-0.048 ± 0.007	0.037 ± 0.010	0.027 ± 0.009	0.029 ± 0.002
$\Delta G^{0'}$ (kcal mol ⁻¹) ⁱ	7.4 ± 0.2	9.4 ± 0.3	9.1 ± 0.2	9.2 ± 0.05
$\lambda (\text{kcal mol}^{-1})^j$	40	12	ND	ND

^a All values derived from measurements made at 298 K and pH 9.8.

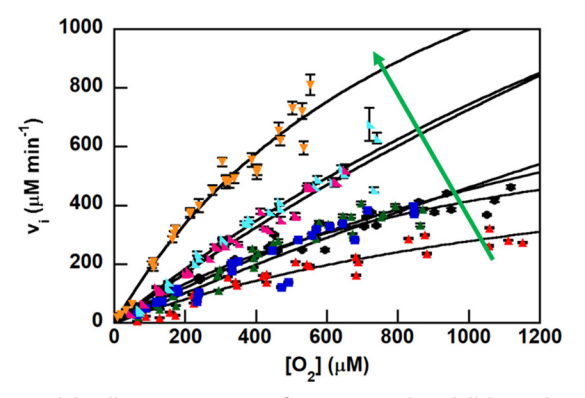


Figure 4. Michaelis-Menten curves for NMO-catalyzed dithranol oxidation at varying temperatures. Initial rates for dithranol oxidation in the presence of 4 μ M NMO in buffer (CAPS-ME, pH 9.8) were measured as a function of O₂ concentration and fit to the Michaelis–Menten equation (Equation 9). Dithranol⁻ was saturating ($\geq 5 \times K_m$) at 500 μ M, and the O₂ consumption was monitored via O_2 electrode with respect to $[O_2]$ at 5 (red triangles), 10 (black circles), 15 (green triangles), 20 (blue squares), 25 (teal right angles), 30 (pink angles), and 37 °C (orange inverted triangles). As expected, the rate increases with increasing temperature (represented by the arrow). Error bars represent the error in the slope from the linear regressions of three or more

form the dithranyl radical were measured for free dithranol and the NMO-dithranol complex using cyclic voltammetry (CV) (Fig. 5 and Fig. S7). Using Equation 11 and $k = 2.6 \times 10^9$ $\mathrm{M}^{-1}\,\mathrm{s}^{-1}$, the dimerization rate constant that has been applied to describe coupling by several other phenolic radicals (20), allowed for the calculation of E^{0} , the redox potential under standard conditions at constant pH (25 °C, 1 M ionic concentration, pH 9.8) for bound and unbound dithranol (Table 1). The presence of NMO does not significantly change E^{0} . These values are reported versus Ag/AgCl (in 3 M NaCl) instead of versus SHE, because there was no suitable redox system for our mixed solvent system that could be used to account for the junction potential. Prior studies have used a correction factor for this in both aqueous (21) and mixed solvent systems (22). However, caution should be taken when doing so, especially if an organic solvent is used (23, 24). To reference the dithranol oxidation to the half-cell potential of $O_2 + e^- \rightarrow O_2^-$, we applied the correction factor below.

$$E_{SHE}^{0'} = E_{Ag/AgCI}^{0'} + 0.209 \text{ V at 25 °C}$$
 (Eq. 1)

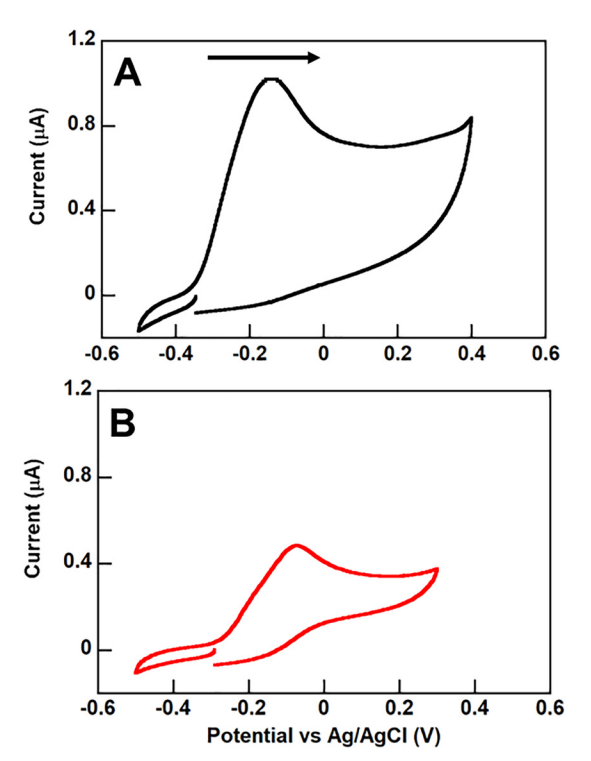


Figure 5. E^{0} and ΔG^{0} for free and NMO-bound dithranol have similar values. CV was run using 1 mm dithranol (A) and 1 mm NMO-dithranol (B) complex in air-saturated buffer (CAPS-ME, 30% (v/v) glycerol, pH 9.8) at 25 °C. The arrow indicates the scan direction (in the oxidative direction). $E_{\rm p}$, the potential where the current reaches a maximum, was used in Equation 11 to determine the standard cell redox potential of dithranol oxidation. E⁰ for free and bound dithranol $^-$ - 0.048 \pm 0.007 and \pm 0.037 \pm 0.01 V, respectively. To calculate the standard free energy of electron transfer from dithranol $^-$ to O $_2$, Equation 10 was used: $\Delta G^{0'}$ free dithranol $^-$ = 7.4 \pm 0.2 and bound dithranol $= 9.4 \pm 0.3$. Binding the substrate to WT NMO makes the reaction more endothermic by 2.0 kcal mol^{-1} .

 $E_{\rm SHE}^{0'}$ for ${\rm O_2}+e^-\to{\rm O_2^-}$ is -0.16 V (5). We then used Equation 10 to solve for $\Delta G^{0'}$ of electron transfer to ${\rm O_2}$ for unbound and bound dithranol (Table 1). There was only a modest increase in the free energy when dithranol is bound to NMO. Hence, the presence of NMO causes a small shift in the free energy toward a more endothermic electron transfer.



 $^{^{}b}$ Units of M^{-1} s

^c From Equation 4.

 $^{^{}d}\Delta H^{\ddagger} = \hat{\epsilon_a} - RT.$

 $[^]e$ $\Delta S^{\dagger} = \ln{(A/\kappa Z)} \times k_{\rm B}$ with $\kappa = 1$, $Z = 10^{11}$ m $^{-1}$ s $^{-1}$, and \ln{A} recorded in the table.

 $f \Delta G^{\dagger} = \Delta H^{\dagger} + T \Delta S^{\dagger}.$

g From Equation 10.

^h pH-independent reduction potentials.

From Equation 9 and $E^{\circ}(O_2) = -0.37 \text{ V } vs. \text{ Ag/AgCl.}$ From Equation 1, ΔG^{\oplus} , and $\Delta G^{O'}$ recorded in the table.

Reorganization energy is the major driver for lowering activation energy in NMO

According to Marcus theory, the activation barrier of an electron transfer (ΔG^{\dagger}) can be parameterized via ΔG^{0} for the electron transfer reaction and the reorganization energy (λ) , as shown below.

$$\Delta G^{\ddagger} = \frac{(\lambda + \Delta G^{0})^{2}}{4\lambda}$$
 (Eq. 2)

 λ is defined as the energy required to reorganize the nuclei of substrate, product, and their immediate solvent environment without electron transfer occurring.

For electron transfer from dithranol to O₂, the activation barrier is 14 kcal mol⁻¹; however, in the presence of WT NMO, the barrier is lowered to 9.2 kcal mol⁻¹. Using the measured values for ΔG^0 , ΔG^{\dagger} , and Equation 2, the reorganization energy is 40 kcal mol⁻¹ for the reaction between O₂ and dithranol⁻, and 12 kcal mol⁻¹ for the NMO- dithranol⁻ complex (Table 1). Hence, NMO acts to lower the activation barrier of rate-limiting electron transfer via a 28 kcal mol⁻¹ shift in the reorganization energy.

Note that, because the Marcus Equation 2 is a second-order polynomial in λ , there are two real, positive solutions, λ_{low} and λ_{high} , for a given $\Delta G^{\dagger} > \Delta G^{0}$. When $\Delta G^{\dagger} = \Delta G^{0}$, there is no kinetic barrier to reaction, and any change to the reorganization energy (for which there is only one solution) increases ΔG^{\dagger} . Therefore, λ_{high} represents the normal case in which ΔG^{\dagger} is proportional to λ and ΔG^0 and where an increase in the driving force for an electron transfer corresponds to an increase in rate. $\lambda_{
m low}$ represents the counterintuitive case where the chemical environment lowers ΔG^{\dagger} for electron transfer by increasing the reorganization energy and/or ΔG^0 . This inversion is physically possible; however, the range of ΔE^0 over which a normal (*i.e.* proportional) relationship between ΔG^{\dagger} and λ is predicted by Marcus theory is given by the square root of the product of the two solutions for the reorganization energy, i.e. $\pm \sqrt{(\lambda_{\rm low}\,\lambda_{\rm high})}$. For the parameters in Table 1, the normal ranges were ± 0.32 and ± 0.39 V for the uncatalyzed and catalyzed cases, respectively. This suggests that a normal relationship between ΔG^{\dagger} and λ should exist (37). The values for λ_{high} are therefore reported.

Discussion

O₂ is nature's premiere oxidant: naturally abundant, relatively nontoxic, kinetically challenged, but thermodynamically powerful. O₂-utilizing processes must overcome the intrinsic barriers to O₂ activation, which can be understood in the context of the self-exchange reaction between $O_2^{\overline{}}$ and O_2 (ΔG^{0}) 0 kcal mol⁻¹). Applying the Marcus relationship (Equation 2) to this reaction gives $\Delta G^{\dagger} = \lambda/4$. Using $k_{\rm ET} = 4.5 \pm 1.6 \times 10^2 \, {\rm M}^{-1}$ s^{-1} as an aqueous rate constant for $O_2^{\overline{\cdot}}$ to O_2 electron transfer, Roth and Klinman (5) estimated barriers of $\Delta G^{\dagger} = 11.5$ and $\lambda =$ 46 kcal mol⁻¹. The value for λ was further broken down as the sum of inner-shell ($\lambda_{in} = 16 \text{ kcal mol}^{-1}$) and outer-shell ($\lambda_{out} =$ 30 kcal mol⁻¹) contributions. λ_{in} is defined as the energy needed to change the internal coordinates of the reactant state to the product state, without transfer of the electron. $\lambda_{\rm out}$ is the

energy required for reorganizing the solvent medium from the reactant to the product state, likewise without transfer of the electron. Hence, λ_{out} , or the energy cost for reorganizing the surrounding polar/aqueous medium, dominates the intrinsic barrier for electron transfer to O_2 in the solvent environment.

Marcus theory suggests that proteins can lower the intrinsic barrier to O₂ activation in two ways. First, the protein environment can impose a rigid and structured network of dipoles that preorganize the active site to minimize molecular reorientations during charge transfer (25), thereby lowering λ (λ_{in} + λ_{out}). Second, an enzyme can stabilize the product state, in which an electron has been fully transferred from the substrate to yield $O_2^{\overline{\cdot}}$ or the initial resting state may be destabilized (*i.e.* substrate activation). These effects are observed in ΔG^0 .

A further key component of the biological strategy for O₂ use is the cofactor. O₂-activating enzymes are most often populated with tightly anchored, intrinsically O2-reactive organic or metallocofactors, within an evolutionarily optimized protein active site environment. This obviates the need to produce a wholly unique active site for each O2-dependent reaction; rather, an already optimal protein-cofactor motif efficiently activates O₂, and the remainder of the active site is adapted toward accommodating the oxidation substrate.

Cofactorless oxidases and oxygenases like NMO have only the protein environment itself for O₂ activation; as such, they illustrate what a natural or engineered protein environment may achieve in the absence of the protein-cofactor motif and how. To understand O₂ activation by NMO, we first noted from prior work that the deprotonated, monoanionic substrate (dithranol⁻) reacts with O₂ much more rapidly than its neutral/ protonated counterpart. In the mixed aqueous/organic buffer used throughout this study, the native pK_a for dithranolH \Leftrightarrow dithranol⁻ + H⁺ was previously measured at 7.9 \pm 0.4. Here, the p K_a for the ES complex was shown to be a full pH unit smaller (6.9 \pm 0.2), corresponding to an energetic contribution of $\Delta G^{0'} = 1.4 \text{ kcal mol}^{-1}$. Two conserved active site asparagines, Asn-18 and Asn-63 (Fig. 6), appear to play roles in lowering the p K_a of the bound substrate and are likewise essential for catalysis to occur at an appreciable rate. They are flanked by two water molecules, which may aid in the deprotonation event. Hence, one role of the protein environment is to activate the substrate by deprotonation, a reaction that happens independent of the presence or absence of O₂. A rate-limiting electron transfer was previously demonstrated for the reaction between the NMO-dithranol complex (the predominant species above pH 6.9) and O2, forming a radical pair (17). We therefore examined the energetics of this process here.

The reaction barrier (activation energy, ϵ_a , and the related quantity ΔG^{\dagger}) was measured for both the uncatalyzed and catalyzed conversion of dithranol $^-|O_2|$ to dithranyl $^+|O_2^-|$ via the temperature dependence of the reaction rate. Prior work demonstrated that this reaction proceeds via rate-limiting formation of O_2^{-} (17). We were therefore able to use the second-order rate constant, k, for the uncatalyzed and $k_{cat}/K_m(O_2)$ for the catalyzed reactions. The latter term encompasses all microscopic reaction steps up to and including the rate-limiting step and was used as a surrogate for a second-order rate constant for electron transfer. A similar approach has been used by others



Protein-mediated O2 activation

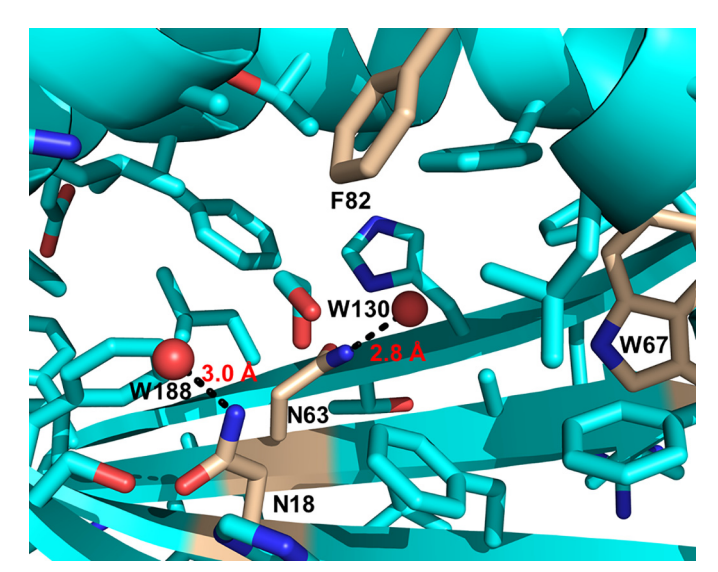


Figure 6. NMO active site pocket has residues that are conserved across the ABM superfamily. The crystal structure of the active site cavity of WT NMO is shown, with ethylene glycol bound (Protein Data Bank code 3KG0). NMO contains a very hydrophobic active site, with several amino acids that are conserved across other members of the ABM superfamily. These include Asn-18, Asn-63, Phe-82, and Trp-67 (17), shown in *gold*. The latter is the only strictly conserved residue among ABMs. Although mutation of this residue results in severely diminished activity (11), its role has yet to be elucidated. Also shown are the two water molecules that flank Asn-18 (Trp-188) and Asn-63 (Trp-130), which are 2.8 and 3.0 Å, respectively; they may play a role in the deprotonation of dithranol and lowering the pK_{σ} .

elsewhere (5, 19). For unbound dithranol⁻, a barrier of ΔG^{\dagger} = 14 kcal mol⁻¹, close to the intrinsic barrier for self-exchange, was measured using the ϵ_a derived from an Arrhenius plot (Fig. 3 and Table 1).

When the dithranol⁻ is part of an NMO-dithranol⁻ complex, the barrier height lowers substantially, to $\Delta G^{\ddagger} = 9.2$ kcal mol⁻¹. The observation of similar pre-exponential factors (A) for both the catalyzed and uncatalyzed processes suggests the electron transfer occurs over a short distance and with similarly high probabilities, whether the reaction occurs inside or outside of the protein environment (26). Hence, the effect of the enzyme is to lower the reaction barrier by \sim 5 kcal mol⁻¹.

To understand how the protein environment does so, we determined the free energy change for the catalyzed and uncatalyzed electron transfer. E^{0} was measured for the dithranol | dithranyl half reaction in buffer and compared with the value measured for the NMO-dithranol complex via a voltammetric method that has previously been used to measure E^{0} for rapidly dimerizing phenolic radicals (20, 27). We previously observed that two dithranyl' rapidly dimerize to form bisanthrone (17). As shown in Table 1, $E^{o'}$ is minimally modulated by the protein environment. The corresponding values of ΔG^{0} for the catalyzed and uncatalyzed reactions, in which dithranol O₂ converts to dithranol O₂, differed by only 2.0 kcal mol⁻¹ (CAPS-ME, pH 9.8, 25 °C). This is comparable in magnitude to the energy required to lower the pK_a of dithranol in the NMO-dithranol complex by 1.0 unit (1.4 kcal mol⁻¹). We concluded that the protein environment had little destabilizing effect on the reactants or stabilizing effects on the products. This is despite the presence of the residues Asn-18 and Asn-63 in proximity to the presumptive substrate-binding site,

which though uncharged could in principle serve to stabilize $O_2^{\overline{}}$ through the resonance form in which the amide side chain has a charge on its nitrogen atom.

The similarity in values of $\Delta G^{0\prime}$ for the catalyzed/uncatalyzed electron transfer suggested that the predominant role of the protein environment is to lower λ , which it does by a sizable 28 kcal mol⁻¹ (Table 1). Notably, both the uncatalyzed and catalyzed reactions between dithranol⁻/O₂ are unaffected by light, indicating that photoexcitation yielding an inner-sphere electron transfer is not at work. We therefore conclude the change in λ is dominated by a lowering of λ_{out} , or outer sphere reorganization of the protein and solvent. In addition, the reaction is pH-dependent, whereas λ_{in} is unaffected by changes in pH (5).

Roth et al. (5, 19) found that glucose oxidase lowers the activation barrier of rate-limiting electron transfer from the flavin cofactor to O_2 via lowering λ_{out} by 19 kcal mol⁻¹. This was accomplished by a single point positive charge in the active site by His-516H⁺, because the effect was eliminated above the histidine's p K_a (5, 19). The catalytic importance of a single positive charge in the active sites of flavoprotein oxidases has been described in numerous examples (28, 29). Although the source of the catalytic effect and its specific assignment to λ has not been studied in enough examples to demonstrate its generality, the conservation of positively charged residues in many flavoprotein oxidases suggests it could be (28). Recently, Olshansky et al. (30) showed that ribonucleotide reductase, which contains a ferric-tyrosyl radical cofactor, catalyzes proton-coupled electron transfer (PCET) via lowering of the reorganization energy by 21 kcal mol⁻¹. PCET must occur between the two subunits, α_2 and β_2 , of ribonucleotide reductase (35 Å apart). It was found that the conformational changes of the α_2 subunit were responsible for enabling PCET and subsequent lowering of λ . These recent studies of electron transfer, along with classic studies of azurin and cytochromes (31-33), all point to the importance of λ in cofactor-dependent proteins.

Conclusions

The NMO protein environment facilitates direct electron transfer from an anionic substrate to O_2 in the absence of a cofactor. Analogous to enzymes that use either an organic or metal-dependent cofactor in a well-evolved active site environment, NMO accelerates rate-limiting electron transfer via lowering of the reorganization energy, where the magnitude of the effect in NMO is robust. This may be a general feature of O_2 -activating enzymes and one that could conceivably be mimicked in engineered proteins.

Experimental procedures

Expression and purification of NMO

The gene encoding the N-terminally ${\rm His}_6$ -tagged NMO (pBad vector) was received as a kind gift from the Schneider laboratory, University of Turku, Turku, Finland. The NMO was expressed and purified as previously described (11). The purified enzyme mass was verified by electrospray ionization MS. Site-directed mutants of NMO were available from a prior study and were expressed and purified using the same protocol as for WT NMO.



Dithranol stocks and reaction media

Dithranol (1,8-dihydroxy-9,10-dihydroanthracen-9-one; MP Biomedicals) was used as a surrogate for the natural NMO substrate, 12-deoxynogalonic acid (Scheme 1). 10 mm stocks were prepared in septum-sealed vials inside an anaerobic chamber (Coy) using DMSO that had been previously rendered anaerobic via multiple cycles of evacuation and purging with Ar. Stock concentrations were verified using the extinction coefficient for dithranol⁻ at pH 9.8, $\epsilon_{387 \text{ nm}} = 18 (\pm 0.2) \text{ mm}^{-1}$ cm⁻¹. The DMSO stock was diluted into reaction medium consisting of 1:2 (v/v) buffer:ME. The organic ME component was essential for solubilizing the substrate and product. The buffer contained 0.1 M CAPS, 0.3 M NaCl in doubly distilled H2O, adjusted to pH 9.8.

Titration of the ES complex

All pH titrations were performed by a discontinuous method using a different buffer for each pH because of instability of the enzyme when concentrated acid or base is added. Titrations of free dithranol and its NMO complex were performed in a Coy anaerobic chamber using an HP8453 spectrophotometer. 100 μM dithranol or 50 μM NMO-dithranol complex (WT, N18A, or N63A) was incubated in various buffers (below) for 3 min before the absorbance was measured. The pK_a was determined by plotting the absorbance at 354 nm (decreasing) and 440 nm (increasing) as a function of pH and fitting the data to a curve describing a single pK_a transition,

$$v = (B \times 10^{-pH} + A \times 10^{-pK_a})/(10^{-pH} + 10^{-pK_a})$$
 (Eq. 3)

where A and B are the highest and lowest absorbance values, respectively.

Buffers at varying pH were prepared as follows: citric acid/ trisodium citrate (pH 5.5, 6.0), BES (pH 6.5, 7.0, 7.5), Tricine (pH 8.0, 8.5), CHES (pH 9.0), and CAPS (pH 10.0, 11.0). Before adjustment to the desired pH with HCl or NaOH, ME was added to each of the 10 solutions, consisting of 100 mm buffer and 300 mm NaCl, to a final concentration of 36% v/v.

Determination of the activation energy (ϵ_a) for the nonenzymatic reaction

The Arrhenius equation quantifies the exponential relationship between a rate constant (k) and temperature (T), with the activation energy ϵ_{a} in the exponential term as follows.

$$k = Ae^{-\epsilon_a/RT} = [\kappa k_B T/h]e^{-\epsilon_a/RT}$$
 (Eq. 4)

Taking the natural logarithm gives the following equation.

$$ln(k) = ln(\kappa k_B T/h) - \epsilon_a/RT$$
 (Eq. 5)

Here $k_{\rm B}$ is the Boltzman constant; h is Planck's constant; R is the universal gas constant; and $\kappa = 1$ if the electron transfer is adiabatic, expected here because the electron donor and acceptor are proximal. The reaction between dithranol and O₂ is expected to be second order, yielding the following rate equation.

$$dithranol^- + O_2 \rightarrow products$$
 (Eq. 6)

rate = $-d[dithranol^{-}]/d[t] = k[dithranol^{-}][O_2]$

(Eq. 7)

The uncatalyzed reaction was monitored under constant concentrations of dissolved O_2 (200 –1200 μ M), maintained via a continuous O₂/N₂ purge. Dissolved [O₂] was measured using a Clark type O₂ electrode (Yellow Springs Instruments) calibrated to air-saturated doubly distilled H2O and corrected for ambient pressure and temperature. dithranol disappearance was monitored discontinuously over time by HPLC (see below) from stirred 2-ml solutions of 460 μ M dithranol in CAPS-ME, pH 9.8. Because the O2 concentration was held constant and only the linear, initial portion of the reaction was monitored, the pseudo-first order and initial rate approximations allowed Equation 7 to simplify to the following,

rate =
$$d[dithranol^{-}]/dt$$
, = $k'[dithranol^{-}]_{initial}$, (Eq. 8)

where k' = k [O₂]. The values for k' were obtained similarly using the method of initial rates in our prior work (17). This allowed us to avoid complications caused by slow reaction times, especially at the lowest temperatures and $[O_2]$.

A line was fitted via least-squares regression to a plot of [dithranol⁻]_t/[dithranol⁻]_{initial} versus time to obtain an initial rate, and Equation 8 was used to solve for k'. A plot of k' versus $[O_2]$ was then used in turn to solve for the slope, k. The values of k measured in this way at a series of temperatures (10–25 °C) were then used to generate an Arrhenius plot. ln (k) versus 1000 R^{-1} T^{-1} was fit to a line by least-squares regression analysis (Kaleidagraph), and ϵ_a was computed from its slope, using Equation 5.

Analysis of reactants and products by HPLC

Quantification of reactants and products was performed on an Agilent 1100 LC system (Agilent Technologies, Santa Clara, CA) equipped with a G1315B diode array detector. Each sample or standard was injected at a volume of 20 µl onto a Hypersil Gold PFP 5 μ m, 4.6 \times 150-mm column (Thermo Scientific) maintained at 50 °C. Buffers used to separate the analytes of interest were 0.1% (v/v) TFA in water (A) and 0.1% (v/v) TFA in acetonitrile (B). The separation was carried out with a gradient: 40% A (0-1 min, 1.5 ml/min), 50% A (1-2 min, 1.5 ml/min), 15% A (2–3 min, 2.0 ml/min), 15% A (3–3.8 min, 2.5 ml/min), 40% A (3.8 – 4.0 min, 1.7 ml/min), and 40% A (4 – 4.1 min, 1.5 ml/min). Analytes were monitored at 354 nm (dithranol), 368 nm (bisanthrone), and 430 nm (dithranone). Integrated intensities of reactant and product were compared against standard curves to determine concentration.

Determination of the activation energy, $\epsilon_{a'}$ for the NMOdithranol - complex

The enzyme-catalyzed oxygenation of dithranol (Equation 6) was previously monitored over time under both single-turnover and steady-state conditions (17). The steady-state kinetic parameter $k_{\text{cat}}/K_m(O_2)$ has been used as a surrogate for the second-order rate constant k (5, 17). This parameter includes all microscopic steps up to and including the rate-limiting step and has the same units as k. We previously showed that k_{cat}



Protein-mediated O2 activation

 $K_m({\rm O}_2)$ and k were close in magnitude (17), where the latter was measured by stopped flow for the reaction between the anaerobic NMO–dithranol $^-$ complex and ${\rm O}_2$. We consequently used the temperature dependence of $k_{\rm cat}/K_m({\rm O}_2)$ for determining the Arrhenius behavior of the NMO-catalyzed reaction here.

Initial rate *versus* substrate concentration plots were generated as a function of $[O_2]$ (80–1200 μ M) using a Clark-type O_2 electrode (Yellow Springs International) in a temperature-controlled chamber (2 ml) with constant stirring. Buffer (CAPS-ME, pH 9.8) was equilibrated with a defined O_2/N_2 gas mixture. Saturating ($\geq 5 \times K_m$) dithranol $\sim (500 \, \mu$ M) was then added, and the linear background O_2 consumption was recorded. After 1 min, 4 μ M NMO was added to initiate the enzymatic reaction, and the consumption of O_2 was monitored. Initial velocities (v_i , Kaleidagraph) of each reaction were fit from the first 5–10% of the progress of reaction curves, corrected for nonenzymatic O_2 consumption. The plot of v_i *versus* $[O_2]$ was fit to the Michaelis–Menten Equation 9 including the effects of cooperativity (H = hill coefficient).

$$v_{i} = \frac{V_{\text{max}}[S]^{H}}{K_{M}^{H} + [S]^{H}}$$
 (Eq. 9)

Values of $\ln k_{\rm cat}/K_m({\rm O_2})$ measured at 5–37 °C were plotted *versus* 1000 R^{-1} T^{-1} and fit to the Arrhenius relationship (Equation 5). Triplicate experiments were performed for each starting $[{\rm O_2}]$.

Measurement of cyclic voltammetry for the uncatalyzed and catalyzed reactions

CV experiments were performed with a SP-50 potentiostat (BioLogic) and EC lab software using a three-electrode cell comprised of a glassy carbon rod encased in polychlorotrifluoroethylene as a working electrode (CH Instruments), and a fritted Ag/AgCl electrode (BASi) as the reference electrode filled with 3 M NaCl (0.209 versus SHE). The working electrodes were prepared immediately prior to each CV by thoroughly polishing on 0.05 μ m alumina powder and sonicating in doubly distilled (Millipore) water for 1 min.

Buffer (CAPS-ME, 30% (v/v) glycerol, pH 9.8) was made anaerobic by alternating argon purges and vacuum cycles and then brought into a Coy anaerobic chamber. Final solutions had a concentration of 30% (v/v) glycerol to keep the enzyme from aggregating. Solutions of either 1 mm dithranol or 1 mm NMO-dithranol complex were prepared in the Coy chamber and transferred with a crimp sealed vial into an electrochemical cell blanketed with argon gas (Airgas UHP 300, 99.999%). Argon was continually passed above the degassed solution during the experiment to create an inert blanket, maintaining anaerobic conditions. All measurements were conducted at 25 °C. The ohmic drop was measured to be less than 200 $\Omega_{\rm s}$ which translated to an iR drop of less than 2 mV for measured currents in the 0.1–1 μ A range. A scan rate of 10 mV s⁻¹ was used to first reduce the solution, followed by an oxidative scan. The irreversible oxidation peak current could then be measured. The potential was referenced against the measured experimental Ag/AgCl potential.

Ag/AgCl calibration

A hydrogen reference electrode (Hydroflex, EDAQ) was placed into a buffered solution (pH 1.68, Oakton) and allowed to soak overnight. A Ag/AgCl electrode (BASi) was placed into the solution and allowed to approach equilibrium for at least 30 min. The potential between the two electrodes was monitored until the drift was less than 1 mV.

Data analysis for determining ΔG^{o}

The Nernst relationship below illustrates how the free energy (ΔG^0) can be determined from the experimentally measured electrochemical potential, where electron transfer to O_2 at pH 9.8 is treated by replacing ΔG^0 with $\Delta G^{0'}$,

$$\Delta G^{0'} = -nF\{E^{0'}[O_2] - E^{0'}[ES, S]\}$$
 (Eq. 10)

where n is the number of electrons (1 in this case), F is Faraday's constant (96,485.33 C/mol), and $E^{0'}$ [ES, S] is the redox potential of dithranol⁻, in the presence (ES) or absence (S) of NMO, and $E^{0'}$ [O₂] is the half-cell reduction potential to reduce O₂ to superoxide. All potentials are expressed as *versus* Ag/AgCl, as a suitable mediator was unable to be found for our mixed solvent system; thus, the junction potential could not be accounted for and referenced to the standard hydrogen electrode.

Phenolic compounds including dithranol are known for their irreversible voltammograms, because of the tendency of the one-electron oxidized species to dimerize (20, 27). The equation for determining phenolic redox potentials, E^0 , in an irreversible one electron oxidation (20) is shown as follows,

$$E_{\rm p} = E^{\rm 0} + \frac{0.902RT}{nF} - \frac{RT}{3nF} \ln \frac{4kC^{\rm 0}RT}{3FV}$$
 (Eq. 11)

where $E_{\rm p}$ is the measured irreversible potential peak, R is the universal gas constant, F is Faraday's constant, n=1, C^0 is the initial [dithranol $^-$], ν is the scan rate, and k describes the dimerization rate constant of bisanthrone formation from two dithranyl radicals. The dimerization constants for phenolic compounds have been approximated to be extremely rapid and near the diffusion limit: $10^9 \, \mathrm{M}^{-1} \, \mathrm{s}^{-1}$ (20). Historically, and in our own stopped-flow experiments (data not shown), anthrone-like compounds are observed to behave similarly to simple phenols (27, 34–36); we therefore used $k=2.6 \times 10^9 \, \mathrm{M}^{-1} \, \mathrm{s}^{-1}$, a value commonly used for phenolic radicals (20).

To determine the effect of the enzyme on the $E^{\prime\prime}$ of dithranol⁻, the difference in the midpoint potential for the substrate (S) and enzyme-substrate (ES) was calculated using the following equation.

$$\Delta E_{\rm ES-S}^{0'} = E_{\rm ES}^{0'} - E_{\rm S}^{0'}$$
 (Eq. 12)

Author contributions—M. M. M. and J. L. D. conceptualization; M. M. M., T. J. C., F. R. B., and J. L. D. resources; M. M. M., E. S. E., and T. J. C. data curation; M. M. M., E. S. E., and T. J. C. formal analysis; M. M. M., F. R. B., and J. L. D. supervision; M. M. M. and E. S. E. investigation; M. M. M., E. S. E., T. J. C., F. R. B., and J. L. D. methodology; M. M. M., E. S. E., and J. L. D. writing-original draft; M. M. M. and J. L. D. project administration; M. M. M., E. S. E., T. J. C., F. R. B., and J. L. D. writing-review and editing; T. J. C., F. R. B., and J. L. D. validation.



Protein-mediated O₂ activation

Acknowledgments-We thank Garrett Moraski; Profs. Robert Szilagyi, Frances Lefcourt, Valérie Copié, and Justine Roth; and Drs. Uma Kaundinya and Ken May for helpful discussions.

References

- 1. Que, L. Q., and Valentine, J. S. (2007) in Biological Inorganic Chemistry: Structure and Reactivity (Gray, H. B., Stiefel, E. I., Valentine, J. S., Bertini, I., eds) pp. 1–40, 1st Ed., University Science Books, Sausalito, CA
- 2. Taube, H. (1965) Mechanisms of oxidation with oxygen. J. Gen. Physiol. **49**, (suppl.) 29 – 52 Medline
- 3. Warren, J. J., Tronic, T. A., and Mayer, J. M. (2010) Thermochemistry of proton-coupled electron transfer reagents and its implications. Chem. Rev. 110, 6961-7001 CrossRef Medline
- 4. Lee, S.-K., and Lipscomb, J. D. (1999) Oxygen activation catalyzed by methane monooxygenase hydroxylase component: proton delivery during the O-O bond cleavage steps. Biochemistry 38, 4423-4432 CrossRef Medline
- 5. Roth, J. P., and Klinman, J. P. (2003) Catalysis of electron transfer during activation of O2 by the flavoprotein glucose oxidase. Proc. Nat. Acad. Sci. U.S.A. 100, 62-67 CrossRef Medline
- 6. Hamdane, D., Zhang, H., and Hollenberg, P. (2008) Oxygen activation by cytochrome P450 monooxygenase. Photosynth. Res. 98, 657-666 CrossRef Medline
- 7. Sirajuddin, S., and Rosenzweig, A. C. (2015) Enzymatic oxidation of methane. Biochemistry 54, 2283-2294 CrossRef Medline
- Chaiyen, P., Fraaije, M. W., and Mattevi, A. (2012) The enigmatic reaction of flavins with oxygen. Trends Biochem. Sci. 37, 373-380 CrossRef Medline
- 9. Miller, A.-F. (2004) Superoxide dismutases: active sites that save, but a protein that kills. Curr. Opin. Chem. Biol. 8, 162-168 CrossRef Medline
- 10. Fetzner, S., and Steiner, R. A. (2010) Cofactor-independent oxidases and oxygenases. Appl. Microbiol. Biotechnol. 86, 791-804 CrossRef Medline
- 11. Grocholski, T., Koskiniemi, H., Lindqvist, Y., Mäntsälä, P., Niemi, J., and Schneider, G. (2010) Crystal structure of the cofactor-independent monooxygenase SnoaB from Streptomyces nogalater: implications for the reaction mechanism. Biochemistry 49, 934-944 CrossRef Medline
- 12. Koskiniemi, H., Grocholski, T., Schneider, G., and Niemi, J. (2009) Expression, purification and crystallization of the cofactor-independent monooxygenase SnoaB from the nogalamycin biosynthetic pathway. Acta Crystallogr. Sect. F Struct. Biol. Cryst. Commun. 65, 256-259 CrossRef
- 13. Adams, M. A., and Jia, Z. (2005) Structural and biochemical evidence for an enzymatic quinone redox cycle in Escherichia coli: identification of a novel quinol monooxygenase. J. Biol. Chem. 280, 8358-8363 CrossRef
- 14. Sciara, G., Kendrew, S. G., Miele, A. E., Marsh, N. G., Federici, L., Malatesta, F., Schimperna, G., Savino, C., and Vallone, B. (2003) The structure of ActVA-Orf6, a novel type of monooxygenase involved in actinorhodin biosynthesis. EMBO J. 22, 205-215 CrossRef Medline
- 15. Kendrew, S. G., Federici, L., Savino, C., Miele, A., Marsh, E. N., and Vallone, B. (2000) Crystallization and preliminary X-ray diffraction studies of a monooxygenase from Streptomyces coelicolor A32 involved in the biosynthesis of the polyketide actinorhodin. Acta Crystallogr. D Biol. Crystallogr. 56, 481-483 CrossRef Medline
- 16. Kendrew, S. G., Hopwood, D. A., and Marsh, E. N. (1997) Identification of a monooxygenase from Streptomyces coelicolor A32 involved in biosynthesis of actinorhodin: purification and characterization of the recombinant enzyme. J. Bacteriol. 179, 4305-4310 CrossRef Medline
- 17. Machovina, M. M., Usselman, R. J., and DuBois, J. L. (2016) Monooxygenase substrates mimic flavin to catalyze cofactorless oxygenations. J. Biol. Chem. 291, 17816-17828 CrossRef Medline

- 18. Verdolino, V., Cammi, R., Munk, B. H., and Schlegel, H. B. (2008) Calculation of p K_a values of nucleobases and the guanine oxidation products guanidinohydantoin and spiroiminodihydantoin using density functional theory and a polarizable continuum model. J. Phys. Chem. B 112, 16860-16873 CrossRef Medline
- 19. Roth, J. P., Wincek, R., Nodet, G., Edmondson, D. E., McIntire, W. S., and Klinman, J. P. (2004) Oxygen isotope effects on electron transfer to O₂ probed using chemically modified flavins bound to glucose oxidase. J. Am. Chem. Soc. 126, 15120-15131 CrossRef Medline
- 20. Li, C., and Hoffman, M. Z. (1999) One-electron redox potentials of phenols in aqueous solution. J. Phys. Chem. B 103, 6653-6656 CrossRef
- 21. Kulys, J., Krikstopaitis, K., and Ziemys, A. (2000) Kinetics and thermodynamics of peroxidase- and laccase-catalyzed oxidation of N-substituted phenothiazines and phenoxazines. J. Biol. Inorg. Chem. 5, 333-340 CrossRef Medline
- 22. O'Reilly, N. J., and Magner, E. (2005) Electrochemistry of cytochrome c in aqueous and mixed solvent solutions: thermodynamics, kinetics, and the effect of solvent dielectric constant. Langmuir 21, 1009-1014 CrossRef
- 23. Pavlishchuk, V. V., and Addison, A. W. (2000) Conversion constants for redox potentials measured versus different reference electrodes in acetonitrile solutions at 25 degrees C. Inorg. Chim. Acta 298, 97-102 CrossRef
- 24. Elgrishi, N., Rountree, K. J., McCarthy, B. D., Rountree, E. S., Eisenhart, T. T., and Dempsey, J. L. (2017) A practical beginner's guide to cyclic voltammetry. J. Chem. Educ. 95, 197-206
- 25. Gray, H. B., and Winkler, J. R. (1996) Electron transfer in proteins. Annu. Rev. Biochem. 65, 537–561 CrossRef Medline
- 26. Moser, C. C., Keske, J. M., Warncke, K., Farid, R. S., and Dutton, P. L. (1992) Nature of biological electron transfer. Nature 355, 796-802 CrossRef Medline
- 27. Roth, H. G., Romero, N. A., and Nicewicz, D. A. (2016) Experimental and calculated electrochemical potentials of common organic molecules for applications to single-electron redox chemistry. Synlett 27, 714–723
- 28. Gadda, G. (2012) Oxygen activation in flavoprotein oxidases: the importance of being positive. Biochemistry 51, 2662-2669 CrossRef Medline
- Visitsatthawong, S., Chenprakhon, P., Chaiyen, P., and Surawatanawong, P. (2015) Mechanism of oxygen activation in a flavin-dependent monooxygenase: a nearly barrierless formation of C4a-hydroperoxyflavin via proton-coupled electron transfer. J. Am. Chem. Soc. 137, 9363-9374 CrossRef Medline
- 30. Olshansky, L., Stubbe, J., and Nocera, D. G. (2016) Charge-transfer dynamics at the α/β subunit interface of a photochemical ribonucleotide reductase. J. Am. Chem. Soc. 138, 1196-1205 CrossRef Medline
- 31. Gray, H. B., and Winkler, J. R. (2009) Electron flow through proteins. Chem. Phys. Lett. 483, 1-9 CrossRef Medline
- 32. Khoshtariya, D. E., Dolidze, T. D., Shushanyan, M., Davis, K. L., Waldeck, D. H., and van Eldik, R. (2010) Fundamental signatures of short- and long-range electron transfer for the blue copper protein azurin at Au/ SAM junctions. Proc. Natl. Acad. Sci. U.S.A. 107, 2757-2762 CrossRef Medline
- 33. Gray, H. B., and Winkler, J. R. (2005) Long-range electron transfer. Proc. Natl. Acad. Sci. U.S.A. 102, 3534-3539 CrossRef Medline
- 34. Nozaki, K., Oyama, M., Hatano, H., and Okazaki, S. (1989) Kinetic study on the dimerization reaction of 9-methoxyanthracene cation radical by means of fast scan cyclic voltammetry. J. Electroanal. Chem. 270, 191-204 CrossRef
- 35. Oturan, M. A., and Y., A. (1984) Mechanism and kinetics of the dimerization of 9-cyanoanthracene. J. Electroanal. Chem. 161, 377-383 CrossRef
- 36. Carney, T. J., Collins, S. J., Moore, J. S., and Brushett, F. R. (2017) Concentration-dependent dimerization of anthraquinone disulfonic acid and its impact on charge storage. Chem. Mater. 29, 4801-4810 CrossRef
- 37. Silverstein, T. P. (2012) Marcus theory: thermodynamics CAN control the kinetics of electron transfer reactions. J. Chem. Educ. 89, 1159-1167 CrossRef



How a cofactor-free protein environment lowers the barrier to O₂ reactivity Melodie M. Machovina, Emerald S. Ellis, Thomas J. Carney, Fikile R. Brushett and Jennifer L. DuBois

J. Biol. Chem. 2019, 294:3661-3669. doi: 10.1074/jbc.RA118.006144 originally published online January 2, 2019

Access the most updated version of this article at doi: 10.1074/jbc.RA118.006144

Alerts:

- · When this article is cited
- · When a correction for this article is posted

Click here to choose from all of JBC's e-mail alerts

This article cites 36 references, 8 of which can be accessed free at http://www.jbc.org/content/294/10/3661.full.html#ref-list-1